Lipids (2015) 50:633–645
DOI 10.1007/s11745-015-4027-7

ORIGINAL ARTICLE

Wax Ester Analysis of Bats Suffering from White Nose Syndrome in Europe

Tomáš Řezanka[1] · Ivan Viden[2] · Alena Nováková[1] · Hana Bandouchová[3] · Karel Sigler[1]

Received: 21 November 2014 / Accepted: 28 April 2015 / Published online: 15 May 2015

Abstract The composition of wax esters (WE) in the fur of adult greater mouse–eared bats (*Myotis myotis*), either healthy or suffering from white nose syndrome (WNS) caused by the psychrophilic fungus *Pseudogymnoascus destructans*, was investigated by high-resolution mass spectrometry analysis in the positive ion mode. Profiling of lipid classes showed that WE are the most abundant lipid class, followed by cholesterol esters, and other lipid classes, e.g., triacylglycerols and phospholipids. WE abundance in non-polar lipids was gender-related, being higher in males than in females; in individuals suffering from WNS, both male and female, it was higher than in healthy counterparts. WE were dominated by species containing 18:1 fatty acids. Fatty alcohols were fully saturated, dominated by species containing 24, 25, or 26 carbon atoms. Two WE species, 18:1/18:0 and 18:1/20:0, were more abundant in healthy bats than in infected ones.

Keywords Chiroptera · High-resolution atmospheric pressure chemical ionization analysis · *Pseudogymnoascus destructans* · Wax esters · White nose syndrome · Emerging fungal skin infection

Electronic supplementary material The online version of this article (doi:10.1007/s11745-015-4027-7) contains supplementary material, which is available to authorized users.

✉ Tomáš Řezanka
rezanka@biomed.cas.cz

[1] Institute of Microbiology, Academy of Sciences of the Czech Republic, Vídeňská 1083, 142 20 Prague 4, Czech Republic

[2] Laboratory of Mass Spectrometry, Institute of Chemical Technology Prague, Technická 5, 166 28 Prague 6, Czech Republic

[3] Department of Ecology and Diseases of Game, Fish and Bees, University of Veterinary and Pharmaceutical Sciences Brno, Palackého 1/3, 612 42 Brno, Czech Republic

Abbreviations

APCI	Atmospheric pressure chemical ionization
APCI-MS/MS	Atmospheric pressure chemical ionization-tandem MS
APPI	Atmospheric pressure photoionization
CE	Cholesterol esters
CID	Collision-induced dissociation
DB	Double bond
ESI	Electrospray ionization
FA	Fatty acids
FAl	Fatty alcohols
FT	Fourier transformation
H-ESI	Heated ESI
HPLC/APCI/MS	High-performance liquid chromatography with atmospheric pressure chemical ionization mass spectrometry
FIA	Flow injection analysis
MALDI	Matrix-assisted laser desorption ionization
MRM	Multiple reaction monitoring
PCR	Polymerase chain reaction
PCA	Principal component analysis
MS^2	Tandem MS
ANOVA	Two-way analysis of variance
WE	Wax esters
WNS	White-nose syndrome

Introduction

White-nose syndrome (WNS) is an emerging infectious disease affecting hibernating insectivorous bats. It was first identified in a cave in Schoharie County, NY, USA in 2006 and named for a distinctive fungal growth around

the muzzle and on the wings of hibernating bats [1]. A psychrophilic *Pseudogymnoascus destructans* (formerly *Geomyces destructans*) is the sole cause of the disease [2]. During hibernation, when the body temperature of bats is decreased to the ambient temperatures of the underground hibernacula, the fungal mycelia can grow upon their skin surfaces [1, 2]. Since 2006, WNS has been spreading into the underground hibernacula in the USA and Canada. At the end of the 2013–2014 hibernating season, it has been confirmed in 25 North American states and five Canadian provinces and more than six million deaths within populations of North American bats have been attributed to the disease since 2007 (http://www.whitenosesyndrome.org). Reports from Europe indicated white fungal growth on hibernating bats without associated deaths [3]. According to Puechmaille *et al.* [4] and Pikula *et al.* [5], *P. destructans* infection in hibernating bats in Europe can be associated with sporadic deaths that may remain unrecognized in the hibernaculum. Mortality rates are low and, to date, have not affected the long-term population size of greater mouse-eared bats [6].

While *P. destructans* has been responsible for mass bat mortalities from WNS in North America, its virulence in Europe has been questioned. However, lesions pathognomonic for WNS are common in European bats and may include overwhelming full-thickness fungal growth through the wing membrane equal in severity to reports from North America. Inter-continental differences in the outcome of WNS in bats in terms of morbidity/mortality may, thus, not be due to differences in the pathogen itself and are likely the result of yet unidentified multifactorial determinants. New data do not support the complete resistance hypothesis of European bats to the infection [7]. The Czech data are relevant also for the USA and Canada since the importance of inter-continental comparative studies on susceptibility, fungal load and transmission, total affected wing/body surface area, behavioral and physiological traits, hibernation environment, and interplay between fungal pathogenic mechanisms and host defenses in bat species has already been highlighted. These findings clearly highlight the importance of inter-continental comparative studies on susceptibility, fungal load and transmission, total affected wing/body surface area, behavioral and physiological traits, hibernation environment, and interplay between fungal pathogenic mechanisms and host defenses in bat species.

In mammals, the main production of surface lipids is associated with the sebaceous glands of the skin. Sebaceous glands are associated with hair follicles that secrete predominantly non-polar lipids in the form of sebum on the skin surface. Although it has been studied in detail in relatively few species, it is obvious that it is present in many species, and it differs greatly in the number and nature of the lipid classes produced.

Compared with traditional dermatophytes such as *Microsporum* and *Trichophyton*, which are restricted to the keratinized and epidermal layers of skin, the WNS fungus breaches the basement membrane and invades the living tissues including the dermis. It is also seen to colonize hair follicles, their associated sebaceous glands, and regional connective tissues [7–9]. These histopathological findings make analysis of hair lipids a relevant approach.

Sebum is composed primarily of glycerolipids (such as triacylglycerols), free fatty acids, sterol esters or wax esters (esters of fatty acids with long chain alcohols) as well as ceramides [10]. Its chemical composition is species-specific [11]. Sebum has many functions; it forms part of the innate immune system, has antimicrobial activity, or prevents evaporative water loss through the skin [10]. In humans, as one of the most studied mammals, it was shown to have still more functions [12]. Given that the skin lipids may affect disease processes, identification of differences in the qualitative and quantitative content of these lipids in healthy and diseased bats could be useful for determining the mechanism of infection of bats by the fungus *P. destructans*.

Mass spectrometry is the most important method for structural characterization of all classes of simple and/or complex lipids. Modern soft ionization techniques, i.e., the formation of gas-phase ions without extensive fragmentation, such as matrix-assisted laser desorption ionization (MALDI) or electrospray ionization (ESI) and atmospheric pressure chemical ionization (APCI) allow an analysis of intact lipids.

Wax esters (waxes), structurally simple lipids composed of long-chain fatty alcohols esterified to fatty acids, represent a major lipid class of the skin secretions [13]. The most widely used methods for analysis of intact waxes are gas chromatography coupled with mass spectrometry [14] or high-performance liquid chromatography with atmospheric pressure chemical ionization mass spectrometry (HPLC/APCI/MS) [15]. Lipidomic analysis of wax esters such as $[M + NH_4]^+$, $[M + H]^+$ or $[M + Li]^+$ adducts by MS without chromatographic separation of individual molecular species by chromatography usually with multiple reaction monitoring (MRM) has also been previously reported [16]. The waxes are complex mixtures, which differ in fatty acyl or long chain alcohols.

Soft ionization techniques generate the majority of ions such as $[M + H]^+$, $[M + NH_4]^+$ or $[M^+$, i.e., alkali metal ions (Li, Na, or K)$]^+$ for the positive ion mode, and ions $[M–H]^-$ in the case of the negative ion mode. There are two basic methods of analysis. The first one uses the front-end HPLC apparatus, which separates lipids into subclasses by normal phase, and these are further analyzed by MS, or they can be divided by reversed phase into the molecular species (not always with complete resolution) and then analyzed using the MS (or tandem MS).

We investigated the composition of wax esters in the fur of adult greater mouse–eared bats, both healthy and suffering from white nose syndrome (WNS) by high-resolution mass spectrometry analysis in the positive ion mode in order to find differences in the WE profiles that would relate to the affliction.

Materials and Methods

Animals and Experiment Design

Bats from an abandoned gold mine Kristýna (Kašperské Hory, Bohemian Forest Mountains, Czech Republic) were examined for WNS in the spring of 2014. The Czech Academy of Sciences' Ethics Committee has reviewed and approved Animal Use Protocol No. 169/2011 in compliance with Law No. 312/2008 on Protection of Animals against Cruelty, as adopted by the Parliament of the Czech Republic. Permits for non-lethal bat sampling were issued by the Czech Nature Conservation Agency (01662/MK/2012S/00775/MK/2012, 866/JS/2012, and 00356/KK/2008/AOPK). Capture and handling of bats was performed so as to minimize stress and duration of sampling procedures. Selection of both WNS-positive and WNS-negative adult greater mouse-eared bats (*Myotis myotis*) for the collection of integumentary lipids and clipping of hairs was guided by trans-illumination of their wing membranes with ultraviolet light (wavelength 368 nm) [17]. The most severely WNS-positive males and females exhibited hundreds of pinpoint orange-yellow fluorescent foci consistent with WNS lesions in each wing membrane [17] (cf. Fig. 1Sa) and were positive for *Pseudogymnoascus* (formerly *Geomyces*) *destructans* on real-time polymerase chain reaction identification (PCR) [18]. Moreover, wing-membrane biopsies were taken from each bat for standard histopathology to confirm WNS and evaluate the severity of infection using the 'gold standard' for WNS diagnosis [8] cf. Fig. 1Sb. Biopsy samples were collected using a sterile disposable 4 mm skin biopsy punch (Kruuse, Denmark) from the left thoracic wing membrane. Formalin-fixed samples were embedded in paraffin, cut into 40 serial tissue sections of 5 μm, and stained for fungi with periodic acid–Schiff stain. Microscopic findings were consistent with the histopathological criteria for WNS diagnosis. The most frequent WNS-positive lesions included cupping erosions packed with *P. destructans* hyphae that locally invaded the dermis as described previously in samples in the Czech Republic [7–9]. On the other hand, bats including the WNS-negative groups of males and females were negative for WNS when examined using ultraviolet light fluorescence, PCR, and histopathology. Three bat specimens were sampled and pooled in each group for the wax ester analysis.

Isolation of Wax Esters

Hair of bats (hairs were taken from twelve bats, three healthy females, three healthy males, three infected females, and three infected males, approximately 1.0 g) was removed with scissors, and lipids were isolated. The four samples of hairs were extracted three times for 5 min with 1.5 mL $CHCl_3$. The combined extracts were dried with anhydrous $MgSO_4$, and the solvent was evaporated almost to dryness. Lipids were separated by TLC with a mixture of dichloromethane-methanol-glacial acetic acid (65:15:2, v/v/v). Samples were loaded on a TLC plate manually by a 100-μl micropipette. Scanning was done by a Shimadzu TLC scanner CS-930 in absorbance mode at 225 nm. The signals from the scanner were collected by Data Recorder DR-2 (Shimadzu). Preparative TLC plates were PLC silica gel (60 F254, 2 mm × 20 cm × 20 cm, Merck, Darmstadt, Germany). Band visualization was carried out with orcinol followed by heating (150 °C). Quantification was performed by means of a TLC scanner and calculated using Statistica 9 software. In the preparative mode, the appropriate four bands were scraped off from the preparative plates, eluted by a mixture of dichloromethane-methanol-glacial acetic acid (65:15:2) and evaporated. The composition of wax esters was further identified by mass spectrometry.

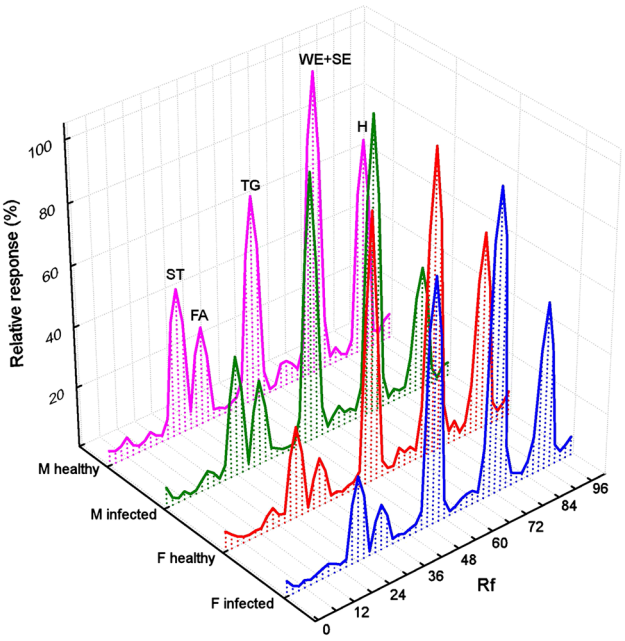

Fig. 1 Quantification of non-polar lipids separated by the TLC scanner and calculated by Statistica 9 software (*M* male, *F* female, *H* hydrocarbons, *WE* + *SE* wax esters + sterol esters, *TG* triacylglycerols, *FA* free fatty acids, *ST* sterols)

Table 1 Relative quantities (%) of molecular species of wax esters identified in bats (male infected, male healthy, female infected, and female healthy), their carbon number(s) and number of double bond(s)

CN	DB	*m/z*	F infected (%)	F healthy (%)	M infected (%)	M healthy (%)
24	1	367.3539	0.0	0.4	0.0	0.0
24	2	365.3422	0.0	0.1	0.0	0.0
24	4	361.3100	0.0	0.1	0.0	0.0
24	5	359.2952	0.0	0.0	0.1	0.0
25	0	383.3892	0.0	0.0	0.0	0.0
25	1	381.3725	0.0	0.2	0.1	0.1
25	2	379.3565	0.0	0.1	0.0	0.0
26	1	395.3892	0.0	0.0	0.2	0.0
26	2	393.3736	0.0	0.2	0.0	0.0
26	3	391.3560	0.0	0.1	0.0	0.0
26	4	389.3422	0.0	0.0	0.0	0.1
26	5	387.3259	0.0	0.2	0.1	0.1
26	6	385.3100	0.0	0.0	0.0	0.1
27	1	409.4076	0.0	0.1	0.0	0.0
27	4	403.3572	0.0	0.2	0.2	0.1
27	5	401.3422	0.0	0.0	1.7	1.0
27	6	399.3263	0.0	0.0	0.0	2.4
28	0	425.4364	0.0	0.0	0.0	0.0
28	1	423.4297	0.3	0.3	0.0	0.0
28	2	421.4036	0.0	0.0	0.0	0.1
28	4	417.3364	1.3	0.1	0.2	0.1
28	5	415.3571	1.7	2.4	2.4	1.2
29	0	439.4145	0.4	0.0	0.0	0.0
29	1	437.4475	0.0	0.2	0.0	0.2
29	4	431.3898	0.1	0.0	0.0	0.1
29	5	429.3728	4.4	6.3	6.4	3.1
29	6	427.3572	0.0	1.1	1.3	0.7
30	0	453.4303	0.6	0.0	0.0	0.0
30	1	451.4511	0.4	0.6	0.9	0.6
30	2	449.4356	0.1	0.0	0.0	0.1
30	3	447.4041	0.2	0.0	0.0	0.0
30	5	443.3887	0.2	0.3	0.0	0.2
30	6	441.3581	0.0	0.2	0.0	0.2
31	0	467.4459	0.5	0.0	0.0	0.0
31	1	465.4670	0.4	0.4	0.6	0.4
31	2	463.3995	1.0	0.1	0.0	0.0
31	3	461.4721	0.1	0.0	0.0	0.0
31	4	459.3833	0.1	0.0	0.0	0.0
31	5	457.4049	0.0	0.0	0.0	0.0
32	1	479.4824	0.7	0.9	1.4	0.9
32	2	477.4667	0.1	0.2	0.2	0.2
32	3	475.4867	0.0	0.0	0.0	0.0
33	0	495.4772	0.2	0.0	0.0	0.0
33	1	493.4980	0.8	1.0	1.0	0.9
33	2	491.4819	0.1	0.4	0.1	0.2
33	3	489.3860	0.0	0.0	0.0	0.0
33	6	483.4051	0.0	0.1	0.0	0.0
34	0	509.5082	0.2	0.0	0.0	0.0
34	1	507.5137	2.5	3.0	2.7	3.2
34	2	505.4980	0.5	0.6	0.9	0.6

Table 1 continued

CN	DB	*m/z*	F infected (%)	F healthy (%)	M infected (%)	M healthy (%)
34	3	503.4831	0.0	0.0	0.0	0.1
34	5	499.5248	0.0	0.0	0.0	0.0
35	0	523.5345	0.1	0.0	0.0	0.0
35	1	521.5291	2.9	0.0	2.8	3.9
35	2	519.5127	0.3	0.4	0.5	0.3
35	3	517.5351	0.4	0.1	0.0	0.1
36	0	537.5364	2.3	0.0	0.0	0.0
36	1	535.5451	9.5	16.3	10.8	17.0
36	2	533.5295	0.9	1.3	1.8	1.2
36	3	531.5129	0.2	0.3	0.4	0.3
36	4	529.4974	0.0	0.0	0.0	0.0
36	5	527.4926	0.0	0.0	0.0	0.0
36	6	525.4774	0.1	0.1	0.3	0.0
37	0	551.5663	0.5	0.0	0.0	0.0
37	1	549.5608	6.5	11.5	6.8	10.2
37	2	547.5448	0.3	0.5	0.6	0.4
37	3	545.5656	0.2	0.0	0.0	0.0
37	5	541.5384	0.1	0.0	0.0	0.0
38	0	565.5672	5.4	0.0	0.0	0.0
38	1	563.5766	9.2	12.4	12.7	13.4
38	2	561.5608	0.6	0.9	1.2	0.8
38	3	559.5445	0.2	0.3	0.3	0.3
38	4	557.5329	0.3	0.3	0.0	0.2
38	5	555.5183	0.2	0.1	0.0	0.0
39	0	579.5984	0.3	0.0	0.0	0.0
39	1	577.5921	4.7	6.1	5.3	5.3
39	2	575.5758	0.2	0.3	0.8	0.3
39	3	573.5614	0.0	0.0	0.0	0.1
39	5	569.5686	0.0	0.0	0.0	0.0
39	6	567.5729	0.5	0.0	0.0	0.0
40	0	593.5985	3.4	0.0	0.0	0.0
40	1	591.6079	5.0	6.5	6.1	5.2
40	2	589.5924	0.4	0.6	0.7	0.6
40	3	587.6500	0.0	0.2	0.3	0.2
40	4	585.5633	0.0	0.1	0.0	0.1
41	0	607.6298	0.2	0.0	0.0	0.0
41	1	605.6235	2.2	2.8	2.3	2.1
41	2	603.6081	0.1	0.3	0.0	0.2
41	4	599.5038	0.4	0.0	0.0	0.0
41	6	595.6040	0.5	0.0	0.0	0.0
42	0	621.6460	0.2	0.0	0.0	0.0
42	1	619.6391	2.4	3.1	2.8	2.4
42	2	617.6245	0.2	0.3	0.3	0.3
42	3	615.6189	0.1	0.0	0.0	0.0
42	4	613.5941	0.1	0.1	0.0	0.1
42	6	609.6184	0.4	0.0	0.0	0.0
43	0	635.6636	0.1	0.0	0.0	0.0
43	1	633.6542	0.7	1.3	0.0	1.0
43	2	631.6216	0.4	0.1	0.0	0.1
43	3	629.5901	0.1	0.0	0.0	0.1

Table 1 continued

CN	DB	*m/z*	F infected (%)	F healthy (%)	M infected (%)	M healthy (%)
43	5	625.6326	0.1	0.0	0.0	0.0
43	6	623.6347	0.3	0.0	0.0	0.0
44	0	649.6780	0.1	0.0	0.0	0.0
44	1	647.6708	1.3	1.7	1.3	1.1
44	2	645.6543	0.1	0.0	0.2	0.3
44	4	641.6274	0.2	0.0	0.0	0.1
44	5	639.6151	0.0	0.1	0.0	0.0
44	6	637.6127	0.1	0.0	0.0	0.0
45	0	663.6856	0.1	0.0	0.0	0.0
45	1	661.6880	0.7	0.9	0.0	0.6
45	2	659.6530	0.3	0.1	0.1	0.2
45	4	655.6436	0.2	0.0	0.0	0.0
45	5	653.6633	0.3	0.0	0.0	0.0
45	6	651.6475	0.6	0.0	0.1	0.0
46	0	677.7045	0.1	0.0	0.0	0.0
46	1	675.7019	1.1	1.5	1.2	0.9
46	2	673.6863	0.4	0.4	1.0	0.9
46	3	671.6661	0.0	0.0	0.0	0.0
46	4	669.6590	0.5	0.6	0.5	0.0
46	5	667.6437	0.3	0.0	0.0	0.0
46	6	665.6282	0.1	0.0	0.1	0.0
47	1	689.7187	0.7	1.0	0.8	0.5
47	2	687.7024	0.3	0.3	0.7	0.6
47	3	685.6540	0.3	0.0	0.0	0.0
47	4	683.6748	0.3	0.4	0.0	0.0
47	6	679.6365	0.1	0.0	0.0	0.0
48	1	703.5727	0.0	1.4	1.0	0.7
48	2	701.7175	1.3	0.7	2.6	2.2
48	4	697.6902	0.5	0.0	0.0	0.0
48	5	695.6763	0.1	0.1	0.0	0.0
48	6	693.6568	0.1	0.0	0.4	0.0
49	1	717.7501	0.5	0.7	0.4	0.3
49	2	715.7333	0.9	0.6	1.3	1.1
49	3	713.7180	0.0	0.0	0.1	0.0
49	4	711.7056	0.1	0.0	0.0	0.0
49	5	709.7257	0.1	0.0	0.0	0.0
49	6	707.7298	0.3	0.0	0.0	0.0
50	1	731.7644	0.0	0.6	0.0	0.0
50	2	729.7490	3.1	1.6	4.7	4.0
50	3	727.7337	0.1	0.1	0.2	0.1
50	4	725.7204	0.0	0.2	0.0	0.0
50	5	723.7077	0.1	0.0	0.0	0.0
51	1	745.7810	0.0	0.3	0.0	0.1
51	2	743.7645	1.1	0.5	1.1	1.0
52	1	759.7953	0.0	0.3	0.0	0.3
52	2	757.7803	2.0	0.6	2.5	1.6
52	3	755.7655	0.0	0.0	0.0	0.0
53	2	771.7957	0.5	0.2	0.6	0.0
54	2	785.8114	0.6	0.0	1.1	0.5
54	5	779.7690	0.0	0.0	0.0	0.0

Table 1 continued

CN	DB	*m/z*	F infected (%)	F healthy (%)	M infected (%)	M healthy (%)
55	2	799.8250	0.2	0.0	0.2	0.0
56	2	813.8421	0.3	0.0	0.3	0.2
58	2	841.8714	0.1	0.0	0.2	0.1
60	1	871.9216	0.0	0.0	0.1	0.0

CN—carbon number, DB—double bond, difference between experimental vs. calculated *m/z* was in the range ± 2.7 ppm

Lipidomic Analysis by HR APCI

The high-resolution hybrid mass spectrometer LTQ Orbitrap Velos (Thermo Scientific, FL, USA) was used. APCI–MS analysis was performed in the positive ion mode. MS spectra were obtained by the FT mode. MS spectra were acquired with target mass resolution of $R = 30{,}000$ at *m/z* 400 [lock mass 391.2842 Da (diisooctyl phtalate)]. The ion spray voltage was set at +2500 V and the scan range of the instruments was set at *m/z* 200–1500. Spray current was 4.0 μA, source temperature was 350 °C, and capillary temperature was 300 °C. Nitrogen was used as a nebulizer gas set at 40 arbitrary units (sheath gas) and 10 arbitrary units (auxiliary gas). Helium was used as a collision gas for CID experiments. The CID normalization energy of 35 % was used for the fragmentation of parent ions. The MS/MS product ions were detected by the low-resolution FT mode. Flow Injection Analysis (FIA) by the pump Accela 650 (Thermo Scientific) was used for sample introduction into the heated APCI ion source. Acetonitrile/methanol (50/50 v/v) was used at the flow rate of 150 μL/min.

Statistics

All experiments were repeated three times. The software Statistica for Windows (version 7.0, Statsoft, Inc., 1984–2004) was used for analyses. All experiments were repeated at least three times. Two different two-way ANOVA analyses were performed to determine significant differences ($p < 0.05$) between male infected, male healthy, female infected, and female healthy bats. The data were presented as simple means (without ±SD), because quantification of numerous lipids containing hundreds of molecular species by high-resolution mass spectrometry on the basis of response factors would require numerous calibration curves obtained by using pure commercially unavailable standards, which would have to be synthesized. Due to these problems, these MS data are preliminary and approximate.

To performing multivariate statistical analyses, we used the program CANOCO 5 (Microcomputer Power, USA). Since the gradient lengths in the data were short, we used a principal component analysis (PCA) to visualize the variability within the dataset.

Results

Analysis

Total lipids were extracted from the hair of bats (male or female, healthy or infected) by a mixture of organic solvents. To reduce the complexity of the non-polar lipids, the extracts were separated by TLC using a solvent mixture of dichloromethane, diethyl ether, and acetic acid to obtain partially purified wax esters. This procedure eliminated most of the other lipid classes from the non-polar lipid extract, especially the abundant triacylglycerols, and only the relevant band corresponding to the wax esters was further analyzed (Fig. 1). Since the wax esters and the steryl esters (SE) cannot be separated properly by TLC, the analytical extract also contains substantial amounts of steryl esters.

There were no differences between the SE fraction in male infected, male healthy, female infected, and female healthy and this fraction was, therefore, not further investigated. Wax esters represented 33 % (male infected), 32 % (male healthy), 38 % (female infected), and 36 % (female healthy) of non-polar lipids.

Tandem mass spectrometry—atmospheric pressure chemical ionization (APCI) was used to determine the structure of wax esters. To evaluate the fragmentation behavior that wax esters exhibit during direct infusion APCI-MS/MS, the product ion mass spectra of six commercially obtained wax ester standards were recorded, viz. 18:0–16:0, 18:1–16:0, 18:0–16:1, 18:1–16:1, 18:2–18:3, and 24:0–24:0 (acid-alcohol), having 34, 36, and 48 total carbon atoms and 0, 1 or 2, and 5 of total DBs as the sum of both acyl and the alcohol moieties. Prior to the fragmentation analysis, we performed full scan analysis of wax esters by APCI in the positive ionization mode.

The fragment pattern that results from soft ionization mass spectrometry of the wax esters strongly depends on the distribution of DBs between the acyl and the alcohol moiety of the molecules. This was confirmed for CID spectra obtained with APCI-MS. We identified the occurrence of four major fragment ions representing the protonated acid ion $[RCOOH_2]^+$, the acylium ion $[RCO]^+$, the dehydrated acylium ion $[RCO\text{-}H_2O]^+$ and the alcohol specific fragment $[R']^+$.

To probe the fragmentation behavior of wax esters during APCI-MS/MS-induced decomposition, we optimized

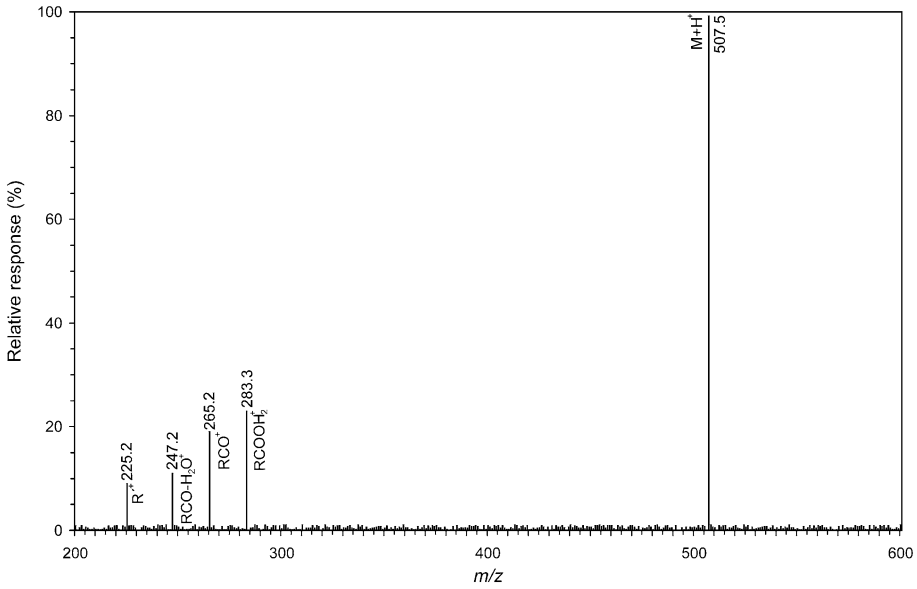

Fig. 2 Tandem mass spectrum of synthetic 18:1–16:0 wax esters

the ionization and fragmentation of our standard wax esters by applying the automated optimization routine of the instrument software. We thus obtained declustering potentials, entrance potentials, and collision energies for the generation of analytical fragments in the mass range from *m/z* 200 to *m/z* 900. The diagnostic acylium fragment ion $[RCO]^+$ and the protonated acid ion $[RCOOH_2]^+$ are found in this mass range; in combination with the precursor mass this allowed the unambiguous identification of the wax esters (Table 1). From the product ion mass spectra and the fragmentation analysis, different wax esters were defined that show characteristic fragment ion spectra. The $[RCOOH_2]^+$ fragment occurs as the predominant diagnostic product ion allowing a sensitive detection of saturated wax esters. Wax esters having one double bond (DB) located in the alcohol moiety reveal the occurrence of a further characteristic fragment ion $[RCO]^+$ that is a predominant product ion. Wax esters with two or three DBs in the alcohol moiety are characterized also by the formation of the important alcohol-derived fragment $[R']^+$. Product ion spectra of wax esters having one DB in the acyl moiety showed the presence of the acylium ion losing water $[RCO\text{-}H_2O]^+$. In wax esters having two or three DBs in the acyl moiety and DBs in the alcohol moiety, the acylium ion $[RCO]^+$ predominates over the other fragment ions. The formation of characteristic product ion spectra according to the distribution of DBs among the alcohol and acyl moiety revealed the same fragmentation rules independent of the overall carbon number of the wax ester, see comparison between 18:0–16:0 and 24:0–24:0, wherein fragmentation and ionization of very long-chain wax esters, i.e., esters above 40 total carbon atoms, decreased.

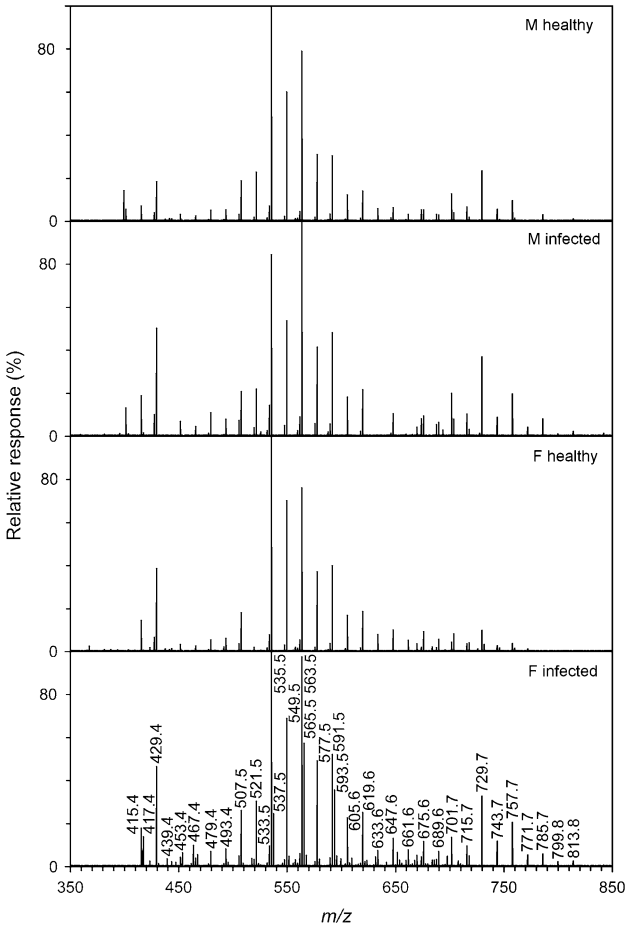

Fig. 3 Mass spectrum (positive ion mode) of non-polar lipids from bats, acquired by high mass resolution APCI-MS. *Numbers* correspond to the accurate mass values

The base peak in the spectrum of wax ester 34:1, i.e., 18:1–16:0 (palmityl oleate), was the ion at *m/z* 507 $[M + H]^+$, see Fig. 2. Further, the spectra contained the ions $[RCOOH_2]^+$ at *m/z* 283, $[RCO]^+$ at *m/z* 265, $[RCO-H_2O]^+$ at *m/z* 247, and $[R']^+$ at *m/z* 225, see Fig. 2.

Speciation of Non-Polar Lipid Classes

Molecular speciation of the major nonpolar lipid class, wax esters (WE), was compared between male infected, male healthy, female infected, and female healthy. The molecular species of WE are shown in Fig. 3. Minor species are not shown, but all species identified are listed in Table 1. Precursor ion scanning allowed identification of fatty acid chain lengths, fatty alcohol chain lengths, and lipid unsaturation. Identification of chain branching, double bond position, and double bond stereochemistry was not pursued in this study.

Wax esters are dominated by species containing 18:1 fatty acids (FA), with such species averaging 28.1 % of the total WE observed. Lower abundance WE included species containing 16:1 (9.8 %), 19:0 (5.4 %), and 26:0 (3.8 %) FA. The fatty alcohols (FAl) observed were fully saturated, dominated by species containing 24, 25, or 26 carbon acyl

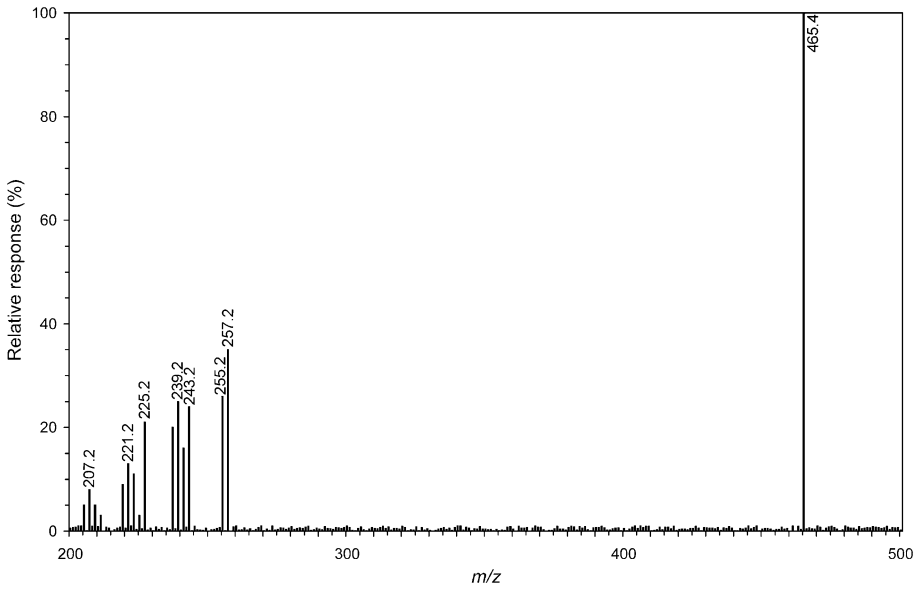

Fig. 4 Tandem mass spectrum of natural 31:1 wax esters

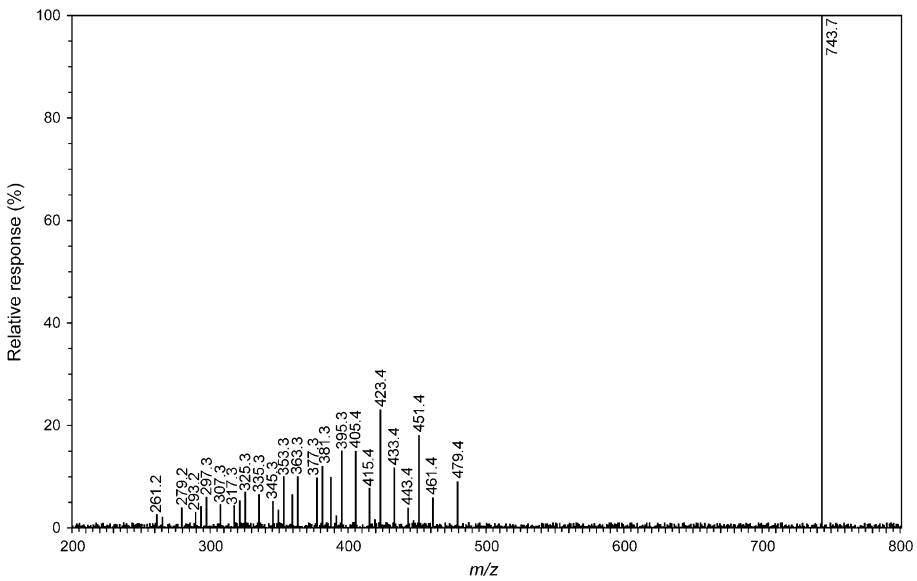

Fig. 5 Tandem mass spectrum of natural 51:2 wax esters

chains (11.3, 8.6, and 5.7 %, respectively). Tandem MS identified fatty acids up to 32 carbon atoms or alcohols up to 35 carbon atoms. Figures 4 and 5 showing tandem MS of 32:1 and 51:2 wax esters illustrate the large number of isobaric molecular species. The values of all identified ions are shown in Table 2 and in Figs. 4 and 5. These data indicate that the ion at 465.5 Da contains four molecular species: 15:1/16:0, 15:0/16:1, 16:1/15:0, and 16:0/15:1 wax ester, whereas the ion at 743.8 Da contains eight molecular species, see Table 1. The most complex ion containing 11 molecular species is at *m/z* 785.8.

A similar pattern of FAl chains was observed for each esterified FA. Great differences were observed in the speciation of abundant WEs between male and female bats.

Table 2 Relative quantities (%) of major molecular species of wax esters identified in bats (male infected, male healthy, female infected, and female healthy), their carbon number(s) and number of double bond(s)

CN-DB	F infected (%)	F healthy (%)	M infected (%)	M healthy (%)
27-5	0.0	0.0	1.7	1.0
28-5	1.7	2.4	2.4	1.2
29-5	4.4	6.3	6.4	3.1
31-2	1.0	0.1	0.0	0.0
32-1	0.7	0.9	1.4	0.9
33-1	0.8	1.0	1.0	0.9
34-1	2.5	3.0	2.7	3.2
35-1	2.9	0.0	2.8	3.9
36-0	2.3	0.0	0.0	0.0
36-1	9.5	16.3	10.8	17.0
36-2	0.9	1.3	1.8	1.2
37-1	6.5	11.5	6.8	10.2
38-0	5.4	0.0	0.0	0.0
38-1	9.2	12.4	12.7	13.4
38-2	0.6	0.9	1.2	0.8
39-1	4.7	6.1	5.3	5.3
40-0	3.4	0.0	0.0	0.0
40-1	5.0	6.5	6.1	5.2
41-1	2.2	2.8	2.3	2.1
42-1	2.4	3.1	2.8	2.4
44-1	1.3	1.7	1.3	1.1
46-1	1.1	1.5	1.2	0.9
46-2	0.4	0.4	1.0	0.9
48-1	0.0	1.4	1.0	0.7
48-2	1.3	0.7	2.6	2.2
49-2	0.9	0.6	1.3	1.1
50-2	3.1	1.6	4.7	4.0
51-2	1.1	0.5	1.1	1.0
52-2	2.0	0.6	2.5	1.6
54-2	0.6	0.0	1.1	0.5

To evaluate the method, a comprehensive wax ester profile of four samples of bats was recorded. The profiles depicting the ten most abundant wax ester species of the male infected, male healthy, female infected, and female healthy are shown in Fig. 3. The two major wax ester species accumulating in the healthy bats were 18:1/16:0 accounting for 10.76 % and 18:1/20:0 accounting for 12.79 % of the total wax ester species. In the infected bats the two species 18:1/16:0 (16.97 %) and 18:1/20:0 (13.41 %) were more abundant. As seen in Figs. 6 and 7, esters with five and six double bonds are relatively abundant, but this is due to the fact that they are cholesterol esters. Cholesterol itself has unsaturation 5 (4 rings and one double bond), so bars marked with five and six double bonds in the graph are, in fact, cholesterol esters of fatty acids having zero or one double bond. We have found no wax ester having five, six, or more double bonds in the molecule, for example, linolenoyl linoleate.

Discussion

Interestingly, with certain exceptions, wax esters of mammals have not been investigated. These exceptions include lanolin (wool fat) [19, 20] or the secretion of meibomian glands in humans [21] or golden hamsters [22]. Far less attention was paid to lipids on the hair of bats.

The non-polar nature of the long hydrocarbon chains of alcohols and fatty acids present in natural waxes forms the basis of their water-repellent properties, which are important for their function as, e.g., natural protectants of human skin and/or animal fur against humidity. Lipids of bats were examined in terms of the content of both lipid classes and the molecular species composition of these classes. Various types of ceramides from *Tadarida brasiliensis* and *Myotis velifer* [10], and triacylglycerols from [23], polar

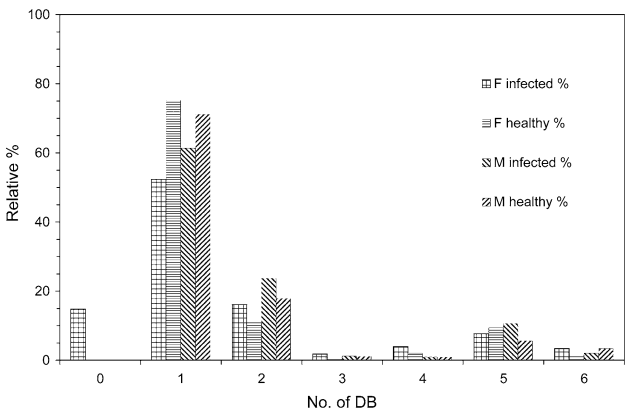

Fig. 6 Ratio of different double bonds of wax esters from hairs of healthy and infected bats of both sexes

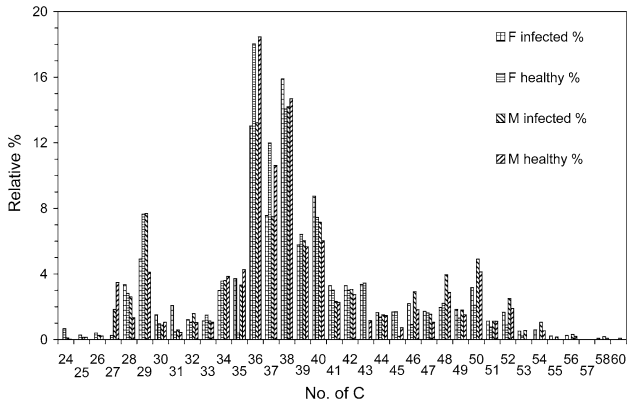

Fig. 7 Ratio of different molecular species of wax esters from hairs of healthy and infected bats of both sexes

lipids from [24], fatty acids [25], and monoacylglycerides, squalene, and sterols always from *Eptesicus fuscus*, *Lasiurus borealis,* and *Nycticeius humeralis* [26] have been reported. With the exception of ceramide [10], no one has yet described in lipid classes of bats the presence of very long chain fatty acids (over 24 carbon atoms), i.e., those that are a normal part of mammalian waxes. We believe that this is mainly due to the use of an experimental technique, since ESI is less suitable for identifying non-polar molecules such as wax esters than APCI or atmospheric pressure photoionization (APPI). The molecular structure of the analyte influences the ionization; ESI is a suitable technique for compounds containing heteroatoms or those that accept a charge by induction. On the other hand, it is not suitable for analyzing strongly non-polar compounds such as wax esters because charge induction in these compounds is not sufficiently efficient. The methods of choice for these compounds are APPI or APCI [27].

Mammals commonly have an acyl-CoA pool consisting of long-chain acyl-CoAs and very long-chain acyl-CoAs from C12 to C32 or more and containing from zero to three double bonds [28]. These acyl chains can either reside in the acyl or the alcohol moiety of the wax ester. Therefore, the number of possibly occurring wax esters may exceed hundreds of molecular species. Rare fatty acids such as odd-chain and methyl-branched fatty acids, commonly found in mammalian waxes, are not included in this calculation [28].

The structure of mammalian wax esters was found to be gender-dependent, see, e.g., the differences between male and female golden hamsters [29] or newborn boys and girls [30]. For example, palmitic acid content in female hamsters was above 40 % total FAs, whereas males did not reach 20 % of total FAs. Similarly, pentadecanoic acid content in males was in tens of a percent, whereas in females it was only up to 2 % of total FAs. In children, it was found that the ratio of wax esters 34:1–38:1 in boys is 1:1.4, while in girls it is the opposite, viz. 0.7:1.

Our data indicate that the composition of wax esters from bats is affected by gender since significant differences were found between the samples from male and female bats, whether healthy or infected. This fact is best reflected in PCA analysis, see Fig. 8, from which it is obvious that

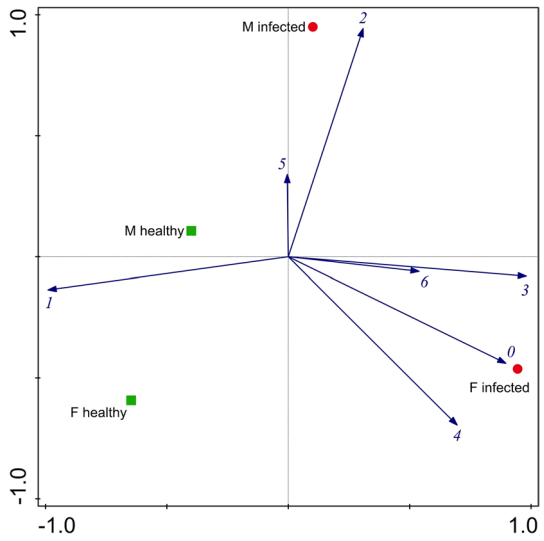

Fig. 8 Principal component analysis (PCA) of the relative proportions of wax esters with a given number of double bonds (*0–5*) in four bat groups (male infected, male healthy, female infected, and female healthy). The first two canonical axes are plotted; the first explained 77.1 % and the second axis 17.9 % of the variability

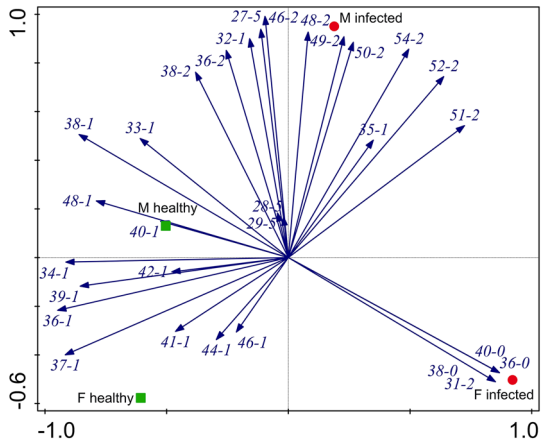

Fig. 9 Principal component analysis (PCA) of the relative proportions of major molecular species of wax esters in four bat groups (male infected, male healthy, female infected, and female healthy). The first two canonical axes are plotted; the first explained 65.4 % and the second axis 14.6 % of the variability. The *numeral in front of the hyphen* is the number of all carbon atoms in the molecule, the *numeral behind the hyphen* is the number of all double bonds in the ester

healthy individuals, regardless of their gender, have hair impregnated with esters with one double bond. As seen clearly in Fig. 8, regardless of the chain length or whether the total number of carbons in the ester is odd or even, wax esters present in healthy individuals are of the type *X*:1 (Fig. 9), where *X* is a number from 24 to 60, i.e., wax esters having one double bond. The cause of this phenomenon is still unclear; however, the melting point of, e.g., 18:0–18:0 is seen to be significantly different from the melting points of 18:1–18:0, 18:0–18:1, and 18:1–18:1 (61.6 °C, 34.0, 23.8 °C, and −4.0 °C, respectively). This can lead to differences in hair lubrication, i.e., hypothetically different efficiency of rubbing the wax into the hair, which can mechanically prevent spore attachment to the body surface.

The presented wax ester profile for bats is in good agreement with previously published data describing fatty acids in hairs of bats, but not alcohols.

Acknowledgments The research was supported by the Czech Science Foundation (Project P506/12/1064) and by the Institutional Research Concept RVO61388971.

References

1. Blehert DS, Hicks AC, Behr M, Meteyer CU, Berlowski-Zier BM, Buckles EL, Coleman JTH, Darling SR, Gargas A, Niver R, Okoniewski JC, Rudd RJ, Stone WB (2009) Bat white nose syndrome: an emerging fungal pathogen? Science 323:227
2. Gargas A, Trest MT, Christensen M, Volk TJ, Blehert DS (2009) *Geomyces destructans* sp. nov. associated with bat white nose syndrome. Mycotaxon 108:147–154
3. Wibbelt G, Kurth A, Hellmann D, Weishaar M, Barlow A, Veith M, Prüger J, Görföl T, Grosche L, Bontadina F, Zöphe U, Seidl HP, Cryan PM, Blehert DS (2010) White-nose syndrome fungus (*Geomyces destructans*) in bats Europe. Emerg Infect Dis 16:1237–1242
4. Puechmaille SJ, Frick WF, Kunz TH, Racey PA, Voigt CC, Wibbelt G, Teeling EC (2011) White-nose syndrome: is this emerging disease a threat to European bats? Trends Ecol Evol 26:570–576
5. Pikula J, Bandouchova H, Novotny L, Meteyer CU, Zukal J, Irwin NR, Zima J, Martinkova N (2012) Histopathology confirms white-nose syndrome in bats in Europe. J Wildl Dis 48:207–211
6. Martinkova N, Backor P, Bartonicka T, Blazkova P, Cerveny J et al (2010) Increasing incidence of *Geomyces destructans* fungus in bats from the Czech Republic and Slovakia. PLoS One 5(11):e13853
7. Bandouchova H, Bartonicka T, Berkova H, Brichta J, Cerny J, Kovacova V, Kolarik M, Kollner B, Kulich P, Martinkova N, Rehak Z, Turner GG, Zukal J, Pikula J (2015) *Pseudogymnoascus destructans*: evidence of virulent skin invasion for bats under natural conditions, Europe. Transbound Emerg Dis 62:1–5
8. Meteyer CU, Buckles EL, Blehert DS, Hicks AC, Green DE, Shearn-Bochsler V, Thomas NJ, Gargas A, Behr MJ (2009) Histopathologic criteria to confirm white nose syndrome in bats. J Vet Diagn Invest 21:411–414
9. Zukal J, Bandouchova H, Bartonicka T, Berkova H, Brack V, Brichta J, Dolinay M, Jaron KS, Kovacova V, Kovarik K, Martinkova N, Ondracek K, Rehak Z, Turner GG, Pikula J (2014) White-nose syndrome fungus: a generalist pathogen of hibernating bats. PLoS One 9(5):e97224
10. Munoz-Garcia A, Ro J, Reichard JD, Kunz TH, Williams JB (2012) Cutaneous water loss and lipids of the stratum corneum in two syntopic species of bats. Comp Biochem Physiol A 161:208–215
11. Nicolaides N, Hwei HC, Rice GR (1968) The skin surface lipids of man compared with those of eighteen species of animals. J Investig Dermatol 51:83–89
12. Smith KR, Thiboutot DM (2008) Sebaceous gland lipids: friend or foe? J Lipid Res 49:271–281
13. Rawlings AV (1995) Skin waxes: their composition, properties, structures and biological significance. In: Hamilton RJ (ed) Waxes: chemistry, molecular biology and functions. The Oily Press, Dundee, pp 223–256
14. Rezanka T, Podojil M (1986) Identification of wax esters of the fresh-water green alga *Chlorella kessleri* by gas chromatography-mass spectrometry. J Chromatogr 362:399–406
15. Rezanka T, Sigler K (2006) Identification of very long chain fatty acids from sugar cane wax by atmospheric pressure chemical ionization liquid chromatography-mass spectroscopy. Phytochemistry 67:916–923
16. Fitzgerald M, Murphy RC (2007) Electrospray mass spectrometry of human hair wax esters. J Lipid Res 48:1231–1246
17. Turner GG, Meteyer CU, Barton H, Gumbs JF, Reeder DM, Overton B, Bandouchova H, Bartonicka T, Martinkova N, Pikula J, Zukal J, Blehert DS (2014) Non-lethal screening of bat wing skin using UV fluorescence to detect lesions indicative of white-nose syndrome. J Wildl Dis 50:566–573
18. Muller LK, Lorch JM, Lindner DL, O'Connor M, Gargas A, Blehert DS (2013) Bat white nose syndrome: a real-time TaqMan polymerase chain reaction test targeting the intergenic spacer region of *Geomyces destructans*. Mycologia 105:253–259
19. Motiuk K (1978) Wool wax acids: a review. J Am Oil Chem Soc 56:91–97
20. Motiuk K (1978) Wool wax-alcohols: a review. J Am Oil Chem Soc 56:651–658
21. Chen J, Green KB, Nichols KK (2013) Quantitative profiling of major neutral lipid classes in human meibum by direct infusion electrospray ionization mass spectrometry. Invest Ophthal Vis Sci 54:5730–5753
22. Harvey DJ, Tiffany JM, Duerden JM, Pandher KS, Mengher LS (1987) Identification by combined gas chromatography-mass spectrometry of constituent long-chain fatty acids and alcohols from the meibomian glands of the rat and a comparison with human meibomian lipids. J Chromatogr 414:253–263
23. Pannkuk EL, Gilmore DF, Savary BJ, Risch TS (2012) Triacylglyceride (TAG) profiles of integumentary lipids isolated from three bat species determined by matrix-assisted laser desorption–ionization time-of-flight mass spectrometry (MALDI–TOF MS). Can J Zool 90:1117–1127
24. Pannkuk EL, Mcguire LP, Gilmore DF, Savary BJ, Risch TS (2014) Glycerophospholipid analysis of eastern red bat (*Lasiurus borealis*) hair by electrospray ionization tandem mass spectrometry. J Chem Ecol 40:227–235
25. Pannkuk EL, Fuller NW, Moore PR, Gilmore DR, Savary BJ, Risch TS (2014) Fatty acid methyl ester profiles of bat wing surface lipids. Lipids 49:1143–1150
26. Pannkuk EL, Gilmore D, Fuller N, Savary BJ, Risch TS (2013) Sebaceous lipid profiling of bat integumentary tissues: quantitative analysis of free fatty acids, monoacylglycerides, squalene, and sterols. Chem Biodivers 10:2122–2132
27. Naegele E (2011) Making your LC method compatible with mass spectrometry. Technical overview. Agilent Technologies, Inc. http://www.chem.agilent.com/Library/technicaloverviews/Public/5990--7413EN.pdf. Accessed 11 May 2015

28. Hamilton RJ (ed) (1995) Waxes: chemistry, molecular biology and functions. Oily Press, Dundee
29. Seyama Y, Otsuka H, Ohashi K, Vivienroels B, Pevet P (1995) Sexual dimorphism of lipids in Harderian glands of golden hamsters. J Biochem 117:661–670
30. Mikova R, Vrkoslav V, Hanus R, Hakova E, Habova Z, Dolezal A, Plavka R, Coufal P, Cvacka J (2014) Newborn boys and girls differ in the lipid composition of vernix caseosa. PLoS One 9(6):e99173